Check for updates

Pan-cancer analysis and experimental verification of its roles and clinical significance of SLC2A3 in kidney renal clear cell carcinoma

Zhaojie Lyu[1*†], Xueqi Zhang[2†], Haichao Yuan[1],
Qingshan Yang[1], Yu Yang[1], Zhengping Zhao[1],
Guangsuo Wang[3,4*] and Liangkuan Bi[1*]

[1]Department of Urology, Institute of Precision Medicine, Peking University Shenzhen Hospital,
Shenzhen, China, [2]Department of Urology, Shenzhen People's Hospital, The Second Clinical Medical
College, Jinan University, Shenzhen, China, [3]Department of Thoracic Surgery, Shenzhen People's
Hospital, The Second Clinical Medical College, Jinan University, Shenzhen, China, [4]The First Affiliated
Hospital, Southern University of Science and Technology, Shenzhen, China

Background: Solute carrier family 2 member 3 (SLC2A3), a key glucose transporter, has been implicated in tumor metabolism and immune regulation, but its specific role in kidney renal clear cell carcinoma (KIRC) remains largely unclear.

Methods: We conducted a comprehensive pan-cancer analysis of SLC2A3 using publicly available datasets. Its associations with patient prognosis, genomic heterogeneity, stemness features, immune-related genes, and immune cell infiltration were systematically explored. Functional enrichment and gene set enrichment analyses (GSEA) were conducted to explore the potential biological mechanisms in KIRC. Additionally, *in vitro* experiments using HK-2 and 786-O cell lines were carried out to validate the functional effects of SLC2A3.

Results: SLC2A3 expression was altered in multiple cancers, being upregulated in eight tumor types and downregulated in twenty. Elevated SLC2A3 levels were associated with poorer survival in several malignancies. SLC2A3 expression is broadly positively correlated with immune checkpoints, modulators, and several immune cells in most cancers, but shows a negative association in TGCT. In KIRC, differential expression and enrichment analyses suggested involvement of SLC2A3 in hormone regulation, extracellular matrix remodeling, complement activation, and steroid metabolism. GSEA further demonstrated significant enrichment of gene sets involved in key pro-tumorigenic pathways. Functional assays demonstrated that silencing SLC2A3 markedly inhibited cell proliferation and migration in both HK-2 and 786-O cells.

Conclusions: Collectively, our data imply that SLC2A3 serves as an oncogenic driver in multiple cancers, contributing to KIRC progression via the enhancement of pro-tumorigenic pathways.

Introduction

Globally, cancer poses a significant health challenge and remains a leading contributor to morbidity and mortality (1, 2). Epidemiological data indicate that both the incidence and mortality of malignant tumors are rising, posing serious threats to patient survival and quality of life (3, 4). Although molecularly targeted therapies and immune checkpoint inhibitors (ICIs) have made significant progress, their effectiveness remains limited due to high recurrence, acquired resistance, and notable interpatient variability (5). Accumulating evidence indicates that the tumor immune microenvironment (TIME) critically shapes therapeutic response, influencing disease progression, treatment resistance, and patient outcomes through complex tumor–immune interactions (6, 7).

Renal cell carcinoma (RCC), as the leading type of kidney cancer, comprises the bulk of renal malignancies (8). Although tyrosine kinase inhibitors (TKIs) and ICIs are widely employed as standard treatments, the majority of patients eventually experience disease progression and therapy resistance, resulting in suboptimal long-term survival (9–11). A major challenge to achieving durable treatment responses lies in the extensive heterogeneity of RCC, which manifests not only at genetic and metabolic levels but also within its immune microenvironment (12, 13). Recent research has highlighted the solute carrier (SLC) family of transporters as key regulators of cellular metabolism, nutrient transport, and tumor-immune interactions (14, 15). For example, SLC1A5 modulates glutamine metabolism, thereby supporting energy production and biosynthetic processes in cancer cells (16). Similarly, SLC2A1, a prominent glucose transporter, is frequently upregulated in tumors and drives glycolytic reprogramming (17). Notably, SLC2A3 (GLUT3), another crucial glucose transporter, has been associated with enhanced energy metabolism, increased invasiveness, and poor prognosis across multiple malignancies (18–20). However, comprehensive investigations of SLC2A3 in RCC remain scarce, and its precise mechanisms and clinical relevance are yet to be fully clarified.

In this study, we comprehensively analyzed SLC2A3 expression across multiple cancer types and evaluated its potential prognostic significance. Furthermore, we investigated the involvement of SLC2A3 in regulating the TIME and validated its biological effects in renal cancer cells through *in vitro* experiments. Collectively, this study aims to elucidate the functional role of SLC2A3 in the initiation and progression of RCC, providing a basis for identifying novel biomarkers and potential therapeutic strategies.

Materials and methods

Data collection and analysis

Comprehensive pan-cancer RNA-seq data and matched clinical information were acquired from the UCSC Xena database (21). Data processing followed the protocol described in our previous study (22). A sign test was further performed to determine the overall trend of SLC2A3 expression across all included cancer types. Survival analyses were performed using the Sangerbox online tool (23), stratifying patients into high- and low-expression SLC2A3 groups using the median expression as the cutoff. The prognostic impact of SLC2A3 on overall survival (OS), disease-specific survival (DSS), progression-free interval (PFI), and disease-free interval (DFI) was evaluated using univariate Cox proportional hazards models.

Analysis of genomic heterogeneity and tumor stemness

Tumor heterogeneity was quantified using multidimensional genomic metrics including tumor mutational burden (TMB), mutant-allele tumor heterogeneity (MATH), microsatellite instability (MSI), loss of heterozygosity (LOH), neoantigen load (NEO), and homologous recombination deficiency (HRD) (24, 25). Data were accessed via the GDC portal (https://portal.gdc.cancer.gov/), with variant calling performed using Mutect2 and downstream analysis conducted with the R package "maftools" (26). Six stemness indices were calculated by integrating DNA methylation and transcriptomic profiles: DNA methylation-based stemness score (DNAss), differentially methylated probe-based stemness score (DMPss), enhancer/epigenetic methylation-based stemness score (ENHss), RNA expression-based stemness score (RNAss), epigenetically regulated DNA methylation stemness score (EREG-METHss), and epigenetically regulated RNA expression-based stemness score (EREG.EXPss) (27).

Analysis of immune-related genes and immune-infiltrating cells

The association between SLC2A3 expression and tumor immune features was analyzed using the R package "TCGAplot" for immune-related genes. Tumor microenvironment scores were assessed separately using the ESTIMATE algorithm (28). The relationship between SLC2A3 expression and immune cell infiltration was evaluated using the ssGSEA and CIBERSORT methods (29, 30).

Functional enrichment analysis

Kidney renal clear cell carcinoma (KIRC) patients were stratified into high- and low-SLC2A3 expression groups using the median value, and differentially expressed genes (DEGs) were identified with the "DESeq2" R package (|log2 fold change| > 1, adjusted p < 0.05). Functional enrichment was performed with the "clusterProfiler" package for GO terms and KEGG pathways (31). Gene sets with FDR < 0.25 and |NES| > 1 were considered significant. Additional GSEA using hallmark gene sets from MSigDB was conducted to explore the molecular mechanisms of SLC2A3 in KIRC (32).

Cell culture and transfection

Human renal proximal tubular epithelial cells (HK-2) and renal cell carcinoma cells (786-O) were purchased from Procell (Wuhan, China). HK-2 cells were cultured in Minimum Essential Medium, and 786-O cells in RPMI-1640, each supplemented with 10% fetal bovine serum and 1% penicillin-streptomycin. All cells were maintained at 37 °C in a humidified atmosphere containing 5% CO_2. Short hairpin RNA (shRNA) vectors were delivered into cells using Lipofectamine 3000, following the manufacturer's protocol. Cells were collected 24–48 hours post-transfection for subsequent functional assays or RNA/protein expression analysis. The control group was transfected with the empty vector (shCtrl). The shRNA sequences are listed in Table 1.

RNA extraction and quantitative real-time PCR

Total RNA was isolated from cultured cells using TRIzol reagent (Invitrogen) following the manufacturer's protocol. RNA concentration and purity were assessed with a NanoDrop spectrophotometer. cDNA was synthesized from 1 μg RNA using the PrimeScript RT reagent kit with gDNA Eraser (Takara). Quantitative real-time PCR was performed with TB Green Premix Ex Taq II (Takara) on a QuantStudio 5 system (Applied Biosystems). Relative mRNA expression was determined using the $2^{\wedge}(-\Delta\Delta Ct)$ method and normalized to β-Actin (33). Primer sequences used in this study are presented in Table 2.

Western blot analysis

Cells were disrupted on ice with RIPA buffer (Beyotime) supplemented with 1 mM PMSF and protease inhibitors. Protein concentrations were measured with a BCA assay kit (Beyotime). Equal amounts of protein (20–30 μg) were separated by 10% SDS-PAGE and transferred onto PVDF membranes. Membranes were blocked with 5% non-fat milk in TBST for 1 h at room temperature, then incubated overnight at 4 °C with primary antibodies against SLC2A3 (1:1000, #A5515, Selleck) and β-Actin (1:5000, #20536-1-AP, Proteintech). Following washing, membranes were exposed to HRP-labeled secondary antibodies (1:5000) for 1 h at room temperature, and protein signals were visualized using an ECL detection kit (Thermo Fisher).

Cell counting kit-8 proliferation assay

Cell proliferation was evaluated using the CCK-8 assay (Beyotime) following the manufacturer's instructions. Transfected cells were seeded into 96-well plates at 3×10^3 cells per well in 100 μL complete medium. At 0, 24, 48, 72, 96, and 120 h, 10 μL of CCK-8 reagent was added to each well, followed by 2 h incubation at 37 °C. Absorbance at 450 nm was measured with a microplate reader (Thermo Fisher).

Flow cytometry for cell cycle analysis

Cell cycle distribution was analyzed by propidium iodide (PI, Beyotime) staining and flow cytometry using a BD FACSCanto II flow cytometer (BD Biosciences, USA). Cells were harvested, washed with cold PBS, and fixed in 70% ice-cold ethanol overnight at 4 °C. After washing, cells were treated with RNase A at 37 °C for 30 min and stained with PI in the dark for 30 min at room temperature.

TABLE 1   Sequences of shRNAs targeting human SLC2A3.

shRNA	Sequence (5′→3′)
shCtrl	ACCGGTCCTAAGGTTAAGTCGCCCTCGC TCGAGCGAGGGCGACTTAACCTTAGGTTTTTGAATTC
ShSLC2A3-1	ccggCGGTGCAGATAGATCTGGAAACTCGAGTTTCCAG ATCTATCTGCACCGTTTTTGAATT
ShSLC2A3-2	ccggCTTGGTCTTTGTAGCCTTCTTCTCGAGAAGAAGG CTACAAAGACCAAGTTTTTGAATT

TABLE 2   Primer sequences used for RT-qPCR.

Gene	Direction	Sequence (5′→3′)
SLC2A3	Forward	ATCCTTCCTGAGGACGTGGAG
SLC2A3	Reverse	TATCAGAGCTGGGGTGACCTTC
β-Actin	Forward	CACCATTGGCAATGAGCGGTTC
β-Actin	Reverse	AGGTCTTTGCGGATGTCCACGT

Wound healing assay

Cell migration was assessed using a wound healing assay. Transfected cells were plated in 6-well plates and cultured until reaching full confluence. A linear scratch was created with a sterile 200 μL pipette tip, and detached cells were removed by washing with PBS. Cells were then incubated in serum-free medium, and wound closure was documented at 0 h and 18 h using an inverted phase-contrast microscope (Olympus).

Transwell migration assay

Cell migration was assessed using 24-well Transwell inserts with 8.0 μm pores (Corning). Transfected cells were resuspended in serum-free medium, and 5×10^4 cells in 200 μL were added to the upper chamber. The lower chamber was filled with 600 μL of complete medium containing 10% FBS. After 48 h incubation at 37 °C, non-migrated cells on the upper surface were removed, while migrated cells on the lower surface were fixed with 4% paraformaldehyde for 20 min, stained with 0.1% crystal violet for 15 min, and rinsed with PBS.

Statistical analysis

Statistical analyses were conducted in R (version 4.4.2) with relevant packages. Comparisons among three or more groups were performed using one-way ANOVA when normality and equal variance assumptions were met, or the Mann–Whitney U test otherwise. Differences between two groups were assessed by Student's t-test. Data are presented as mean ± SD, and experiments were repeated three times independently. A two-sided p value < 0.05 was considered statistically significant.

Result

Expression and prognostic significance of SLC2A3 across human cancers

Comparative analysis of tumor and adjacent normal tissues revealed that SLC2A3 expression was significantly upregulated in eight cancer types, including STES, KIPAN, STAD, HNSC, KIRC, PAAD, TGCT, and CHOL. In contrast, SLC2A3 was downregulated in twenty cancer types, including GBMLGG, LGG, UCEC, BRCA, CESC, LUAD, KIRP, COAD, COADREAD, PRAD, LUSC, LIHC, BLCA, THCA, OV, UCS, ALL, LAML, ACC, and KICH (Figure 1A). Prognostic evaluation indicated that elevated expression was linked to poorer OS in 13 cancers, whereas in TARGET-ALL, reduced levels were similarly associated with worse outcomes (Figure 1B). For DSS, high SLC2A3 predicted unfavorable survival in 13 tumor types, while decreased expression correlated with poor prognosis in PRAD (Figure 1C). Regarding DFI, increased expression was detrimental in three cancers

(Figure 1D). Likewise, for PFI, high levels served as a negative prognostic indicator in 11 cancers, whereas in CHOL, low expression predicted worse outcomes (Figure 1E).

Association between SLC2A3 expression and genomic heterogeneity

Correlation analysis indicated a positive association between SLC2A3 expression and TMB across eight cancer types, while a negative correlation was observed in LIHC (Figure 2A). Regarding MATH, significant positive associations were identified in five cancer types, while four exhibited negative correlations (Figure 2B). For MSI, SLC2A3 expression was positively correlated in four tumor types and negatively correlated in five (Figure 2C). Analysis of NEO revealed positive associations in three cancers (Figure 2D). In terms of HRD, elevated SLC2A3 correlated positively in six cancers, but showed negative correlations in GBM and STAD (Figure 2E). Similarly, for LOH, positive correlations were found in seven tumor types, while negative associations were observed in STAD and THCA (Figure 2F).

Association between SLC2A3 expression and tumor stemness

Stemness analysis demonstrated diverse associations between SLC2A3 and stemness indices. In the DNAss score, positive correlations were observed in seven cancers, whereas negative correlations were detected in twelve (Figure 3A). In EREG-METHss, positive and negative associations were found in eight and thirteen cancer types, respectively (Figure 3B). With DMPss, six cancers showed positive correlations and nine showed negative ones (Figure 3C). For ENHss, SLC2A3 expression correlated positively in seven cancers but negatively in twelve (Figure 3D). Similar trends were seen in RNAss, with seven positive and twelve negative associations (Figure 3E). Lastly, in EREG.EXPss, six tumor types demonstrated positive correlations, while seven showed negative ones (Figure 3F).

Association analysis of SLC2A3 expression with immune-related genes in human cancers

To systematically assess the relationship between SLC2A3 and immune-related genes, correlations were analyzed across 33 tumor types. SLC2A3 exhibited a positive correlation with immune checkpoint genes (ICGs) across the majority of cancers, whereas an opposite trend was observed in TGCT (Figure 4A). Similar patterns were observed for immunostimulatory factors (Figure 4B), chemokines (Figure 4C), immunoinhibitors (Figure 4D), and chemokine receptors (Figure 4E), with widespread positive correlations in the majority of tumors and negative correlations specifically in TGCT.
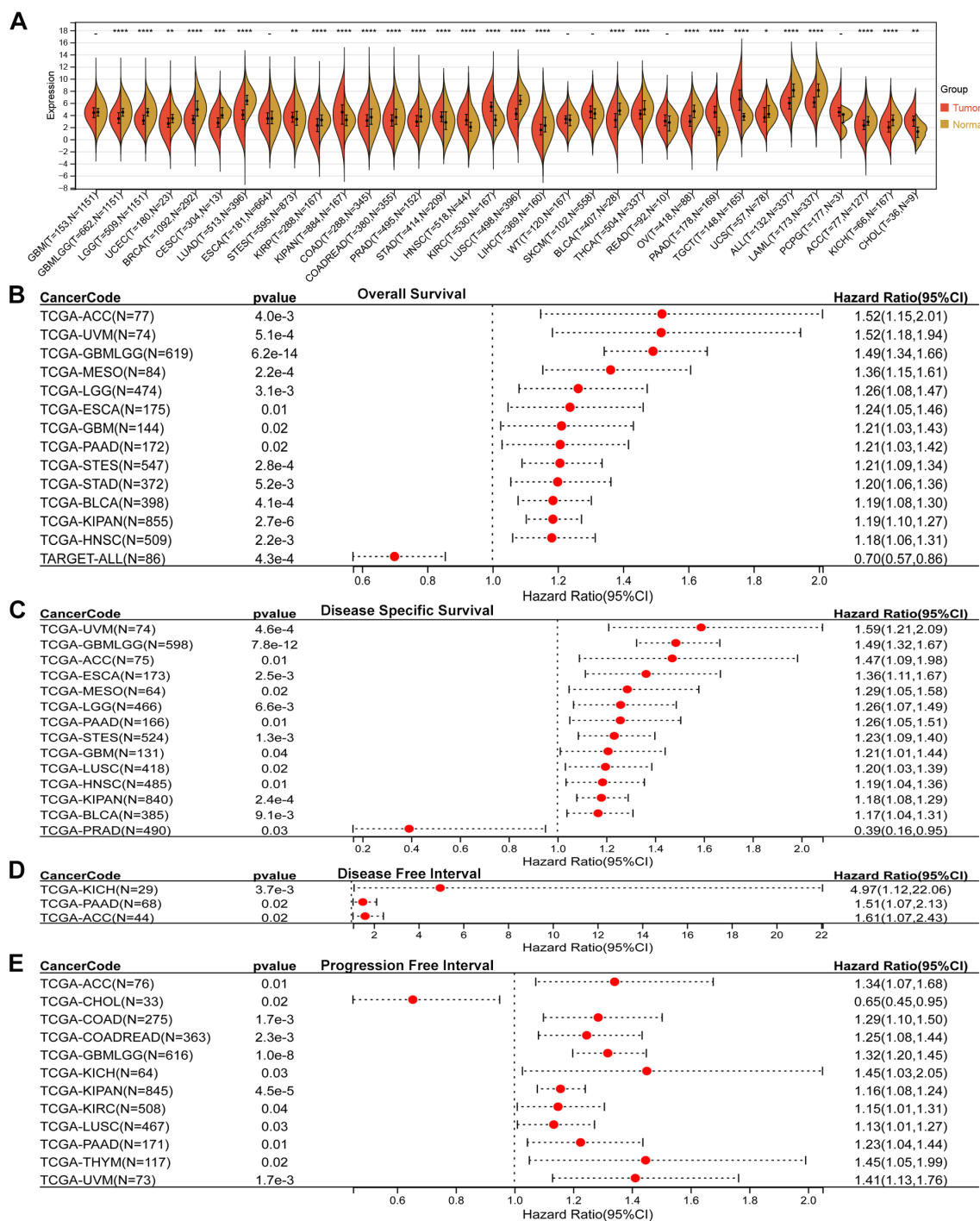
FIGURE 1

Pan-cancer expression and prognostic value of SLC2A3. **(A)** Comparison of SLC2A3 expression between tumor and corresponding normal tissues across multiple cancer types. SLC2A3 was significantly upregulated in eight tumor types and downregulated in twenty tumor types. **(B)** Overall survival (OS) analysis showing that elevated SLC2A3 expression was associated with unfavorable prognosis in thirteen tumor types, whereas reduced expression predicted poor prognosis in TARGET-ALL. **(C)** Disease-specific survival (DSS) analysis indicating that high SLC2A3 expression was linked to poor outcomes in thirteen tumor types, while low expression was associated with worse prognosis in prostate adenocarcinoma (PRAD). **(D)** Disease-free interval (DFI) analysis demonstrating that high SLC2A3 expression correlated with poor prognosis in three tumor types. **(E)** Progression-free interval (PFI) analysis showing that high SLC2A3 expression was related to poor prognosis in eleven tumor types, whereas low expression was associated with adverse outcomes in cholangiocarcinoma (CHOL).
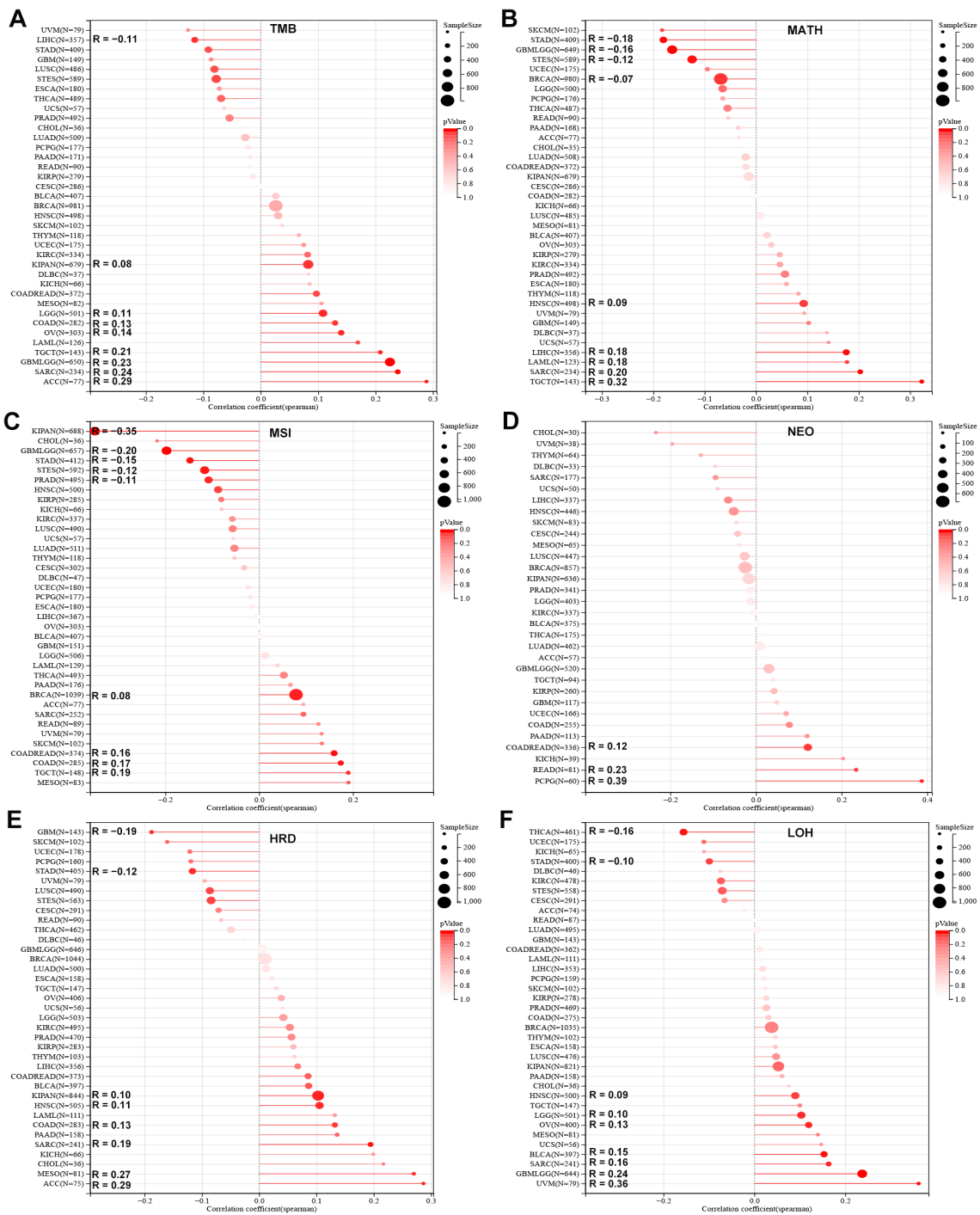
FIGURE 2

Association of SLC2A3 expression with genomic heterogeneity across cancers. **(A)** Correlation between SLC2A3 expression and tumor mutational burden (TMB) across multiple cancer types. **(B)** Correlation between SLC2A3 expression and mutant-allele tumor heterogeneity (MATH) across multiple cancer types. **(C)** Correlation between SLC2A3 expression and microsatellite instability (MSI) across multiple cancer types. **(D)** Correlation between SLC2A3 expression and neoantigen load (NEO) across multiple cancer types. **(E)** Correlation between SLC2A3 expression and homologous recombination deficiency (HRD) across multiple cancer types. **(F)** Correlation between SLC2A3 expression and loss of heterozygosity (LOH) across multiple cancer types.
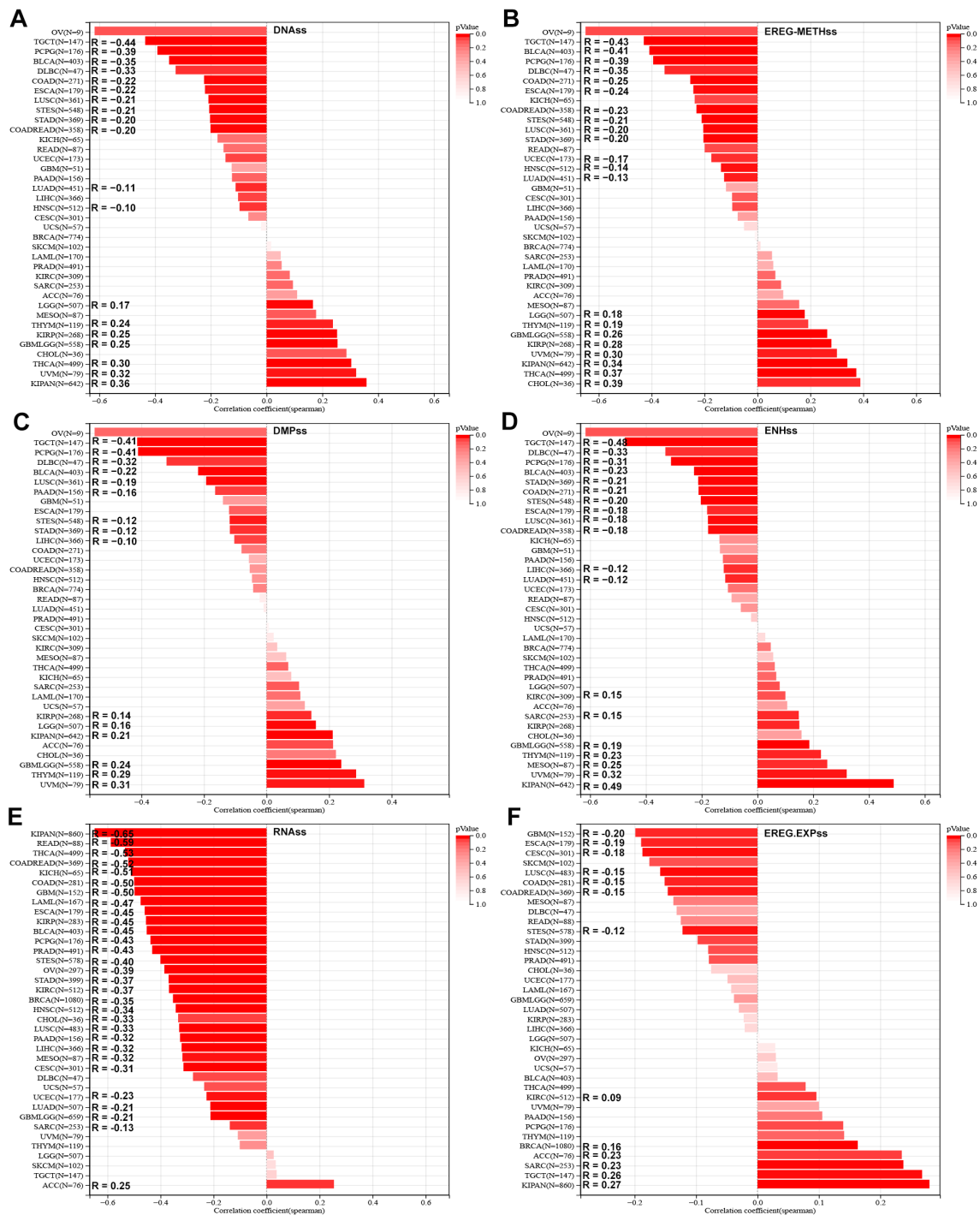
FIGURE 3

Association of SLC2A3 expression with tumor stemness across cancers. **(A)** Correlation between SLC2A3 expression and DNA methylation–based stemness score (DNAss) across multiple cancer types. **(B)** Correlation between SLC2A3 expression and epigenetically regulated methylation–based stemness score (EREG-METHss) across multiple cancer types. **(C)** Correlation between SLC2A3 expression and DNA methylation profile–based stemness score (DMPss) across multiple cancer types. **(D)** Correlation between SLC2A3 expression and enhancer–based stemness score (ENHss) across multiple cancer types. **(E)** Correlation between SLC2A3 expression and RNA–based stemness score (RNAss) across multiple cancer types. **(F)** Correlation between SLC2A3 expression and epigenetically regulated expression–based stemness score (EREG.EXPss) across multiple cancer types.
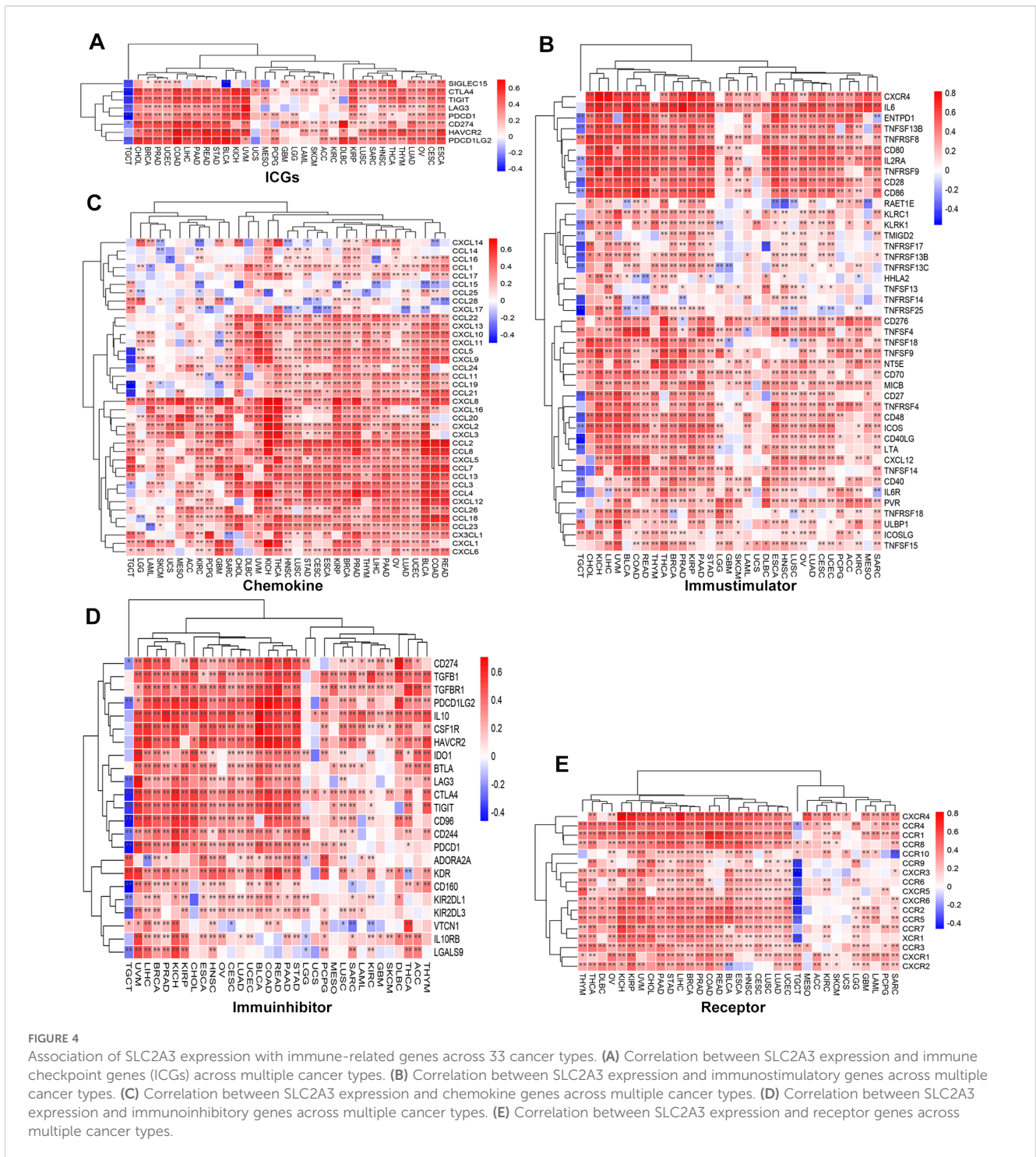
FIGURE 4

Association of SLC2A3 expression with immune-related genes across 33 cancer types. **(A)** Correlation between SLC2A3 expression and immune checkpoint genes (ICGs) across multiple cancer types. **(B)** Correlation between SLC2A3 expression and immunostimulatory genes across multiple cancer types. **(C)** Correlation between SLC2A3 expression and chemokine genes across multiple cancer types. **(D)** Correlation between SLC2A3 expression and immunoinhibitory genes across multiple cancer types. **(E)** Correlation between SLC2A3 expression and receptor genes across multiple cancer types.

Association analysis of SLC2A3 expression with immune-infiltrating cells in human cancers

SLC2A3 was positively correlated with StromalScore, ImmuneScore, and ESTIMATEScore in most cancers, but showed a negative correlation in TGCT and no significant association in ACC, LGG, SKCM, and UCS (Figure 5A). Based on ssGSEA results, SLC2A3 expression was negatively correlated with immune cell infiltration in TGCT but showed no significant association in UCS. In contrast, across most tumor types, SLC2A3 expression demonstrated positive associations with macrophages, helper T cells, Th1, Th2, and regulatory T cells (Tregs), while exhibiting a negative correlation with Th17 cells (Figure 5B). CIBERSORT analysis showed that SLC2A3 expression was positively associated with CD4 memory-activated T cells, M0 macrophages, activated mast cells, and neutrophils, but negatively correlated with regulatory T cells (Tregs), activated NK cells, and memory B cells in most cancers (Figure 5C).
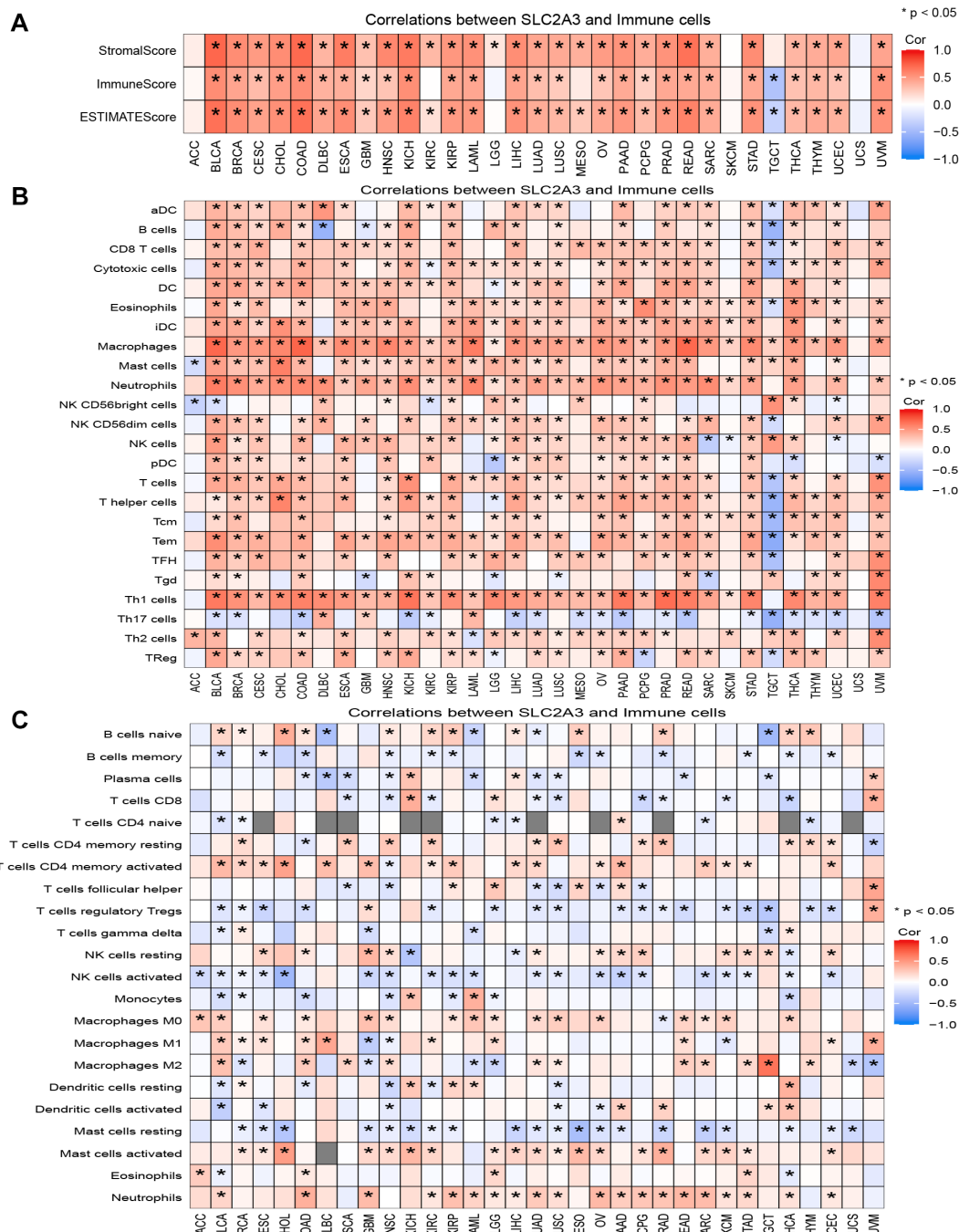
FIGURE 5

Association of SLC2A3 expression with the tumor immune microenvironment across cancers. **(A)** Correlation between SLC2A3 expression and StromalScore, ImmuneScore, and ESTIMATEScore across multiple cancer types. **(B)** Correlation between SLC2A3 expression and immune cell infiltration estimated by ssGSEA across multiple cancer types. **(C)** Correlation between SLC2A3 expression and immune cell infiltration estimated by CIBERSORT across multiple cancer types.

Expression pattern and functional enrichment analysis in KIRC patients

We previously constructed a SLC family-related gene signature for prognosis prediction and confirmed that SLC2A3 is a potential prognostic biomarker for patients with KIRC (19). Unmatched and matched analyses of the TCGA-KIRC dataset demonstrated significant

upregulation of SLC2A3 in KIRC tumors (Figures 6A, B). This finding was further validated by data from UALCAN, which showed elevated promoter methylation of SLC2A3 in normal tissues (Figure 6C). As shown in Figure 6D, a total of 164 genes were significantly upregulated and 630 genes were significantly downregulated in the high SLC2A3 expression group, which were visualized by a volcano plot. A heatmap depicting the top 20 upregulated and downregulated genes is shown in
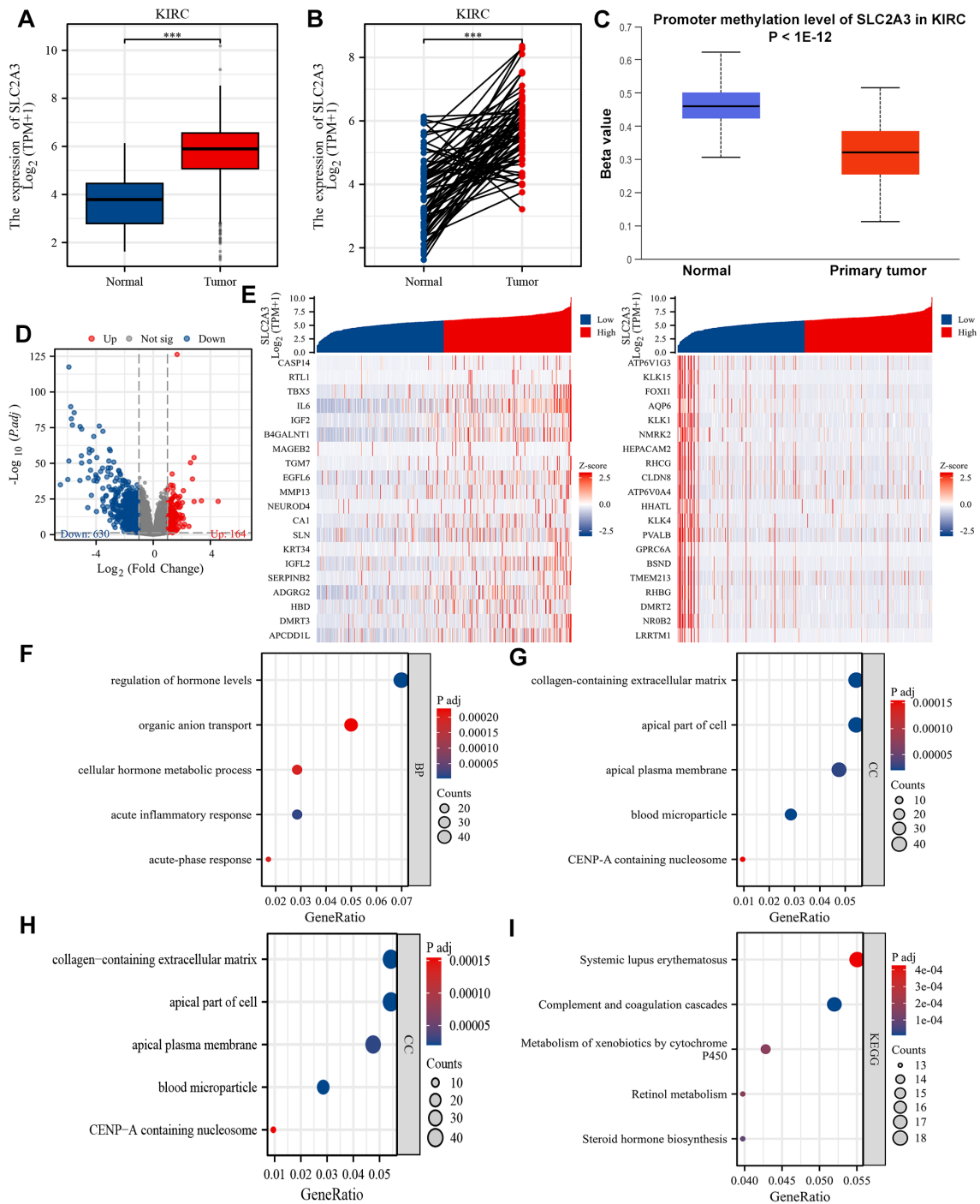
FIGURE 6

Differential expression and functional enrichment analysis based on SLC2A3 expression in KIRC. **(A)** The mRNA expression level of SLC2A3 in the non-matched analysis results of the TCGA-KIRC cohort. **(B)** The mRNA expression level of SLC2A3 in the paired analysis results of the TCGA-KIRC cohort. **(C)** The promoter methylation level of SLC2A3 was obtained from the UALCAN database in the TCGA-KIRC cohort. **(D)** Volcano plot showing 164 upregulated genes and 630 downregulated genes between high and low SLC2A3 expression groups in the TCGA-KIRC cohort. **(E)** Heatmap displaying the top 20 upregulated and downregulated genes. **(F)** Gene Ontology (GO) enrichment analysis of biological process (BP) terms. **(G)** GO cellular component (CC) enrichment. **(H)** GO molecular function (MF) enrichment. **(I)** KEGG pathway enrichment analysis.

Figure 6E. Gene Ontology (GO) biological process (BP) enrichment analysis revealed that the DEGs were primarily associated with regulation of hormone levels, organic anion transport, cellular hormone metabolic process, acute inflammatory response, and acute-phase response (Figure 6F). In terms of cellular component (CC)

enrichment, the genes were significantly enriched in collagen-containing extracellular matrix, apical part of cell, apical plasma membrane, blood microparticle, and CENP-A containing nucleosome (Figure 6G). For molecular function (MF) enrichment, the genes were primarily associated with secondary active

transmembrane transporter activity, serine hydrolase activity, serine-type peptidase activity, serine-type endopeptidase activity, and heparin binding (Figure 6H). Finally, KEGG pathway enrichment analysis revealed that the genes were significantly involved in systemic lupus erythematosus, complement and coagulation cascades, metabolism of xenobiotics by cytochrome P450, retinol metabolism, and steroid hormone biosynthesis (Figure 6I).

GSEA identified four hallmark pathways with significant enrichment. Specifically, Figure 7A shows enrichment of the TNFα signaling via NF-κB pathway, Figure 7B shows enrichment of epithelial-mesenchymal transition (EMT), Figure 7C shows enrichment of inflammatory response, and Figure 7D shows enrichment of the hypoxia pathway.

Functional validation of SLC2A3 in normal renal cell lines and renal tumor cell lines

To explore the function of SLC2A3, functional experiments were conducted in HK-2 and 786-O cells, with knockdown verified

by RT-qPCR and Western blotting (Figures 8A, B). Suppression of SLC2A3 significantly inhibited cell proliferation, as shown by CCK-8 assays (Figure 8C), and reduced the proportion of cells in S phase according to flow cytometry analysis (Figures 8D–F). Additionally, wound healing assays demonstrated markedly impaired migratory capacity in both cell lines following SLC2A3 knockdown (Figure 8G), which was further supported by decreased migration in Transwell assays (Figure 8H). HK-2 cells served as non-malignant renal tubular controls to provide a physiological context for tumor-specific alterations observed in 786-O cells, reflecting the properties of normal proximal tubular epithelium.

Discussion

Recent years have witnessed substantial advances in the development of molecularly targeted therapies and immunotherapies for a wide range of cancers (34, 35). Nevertheless, patients with solid tumors such as RCC still face poor prognosis and frequent drug
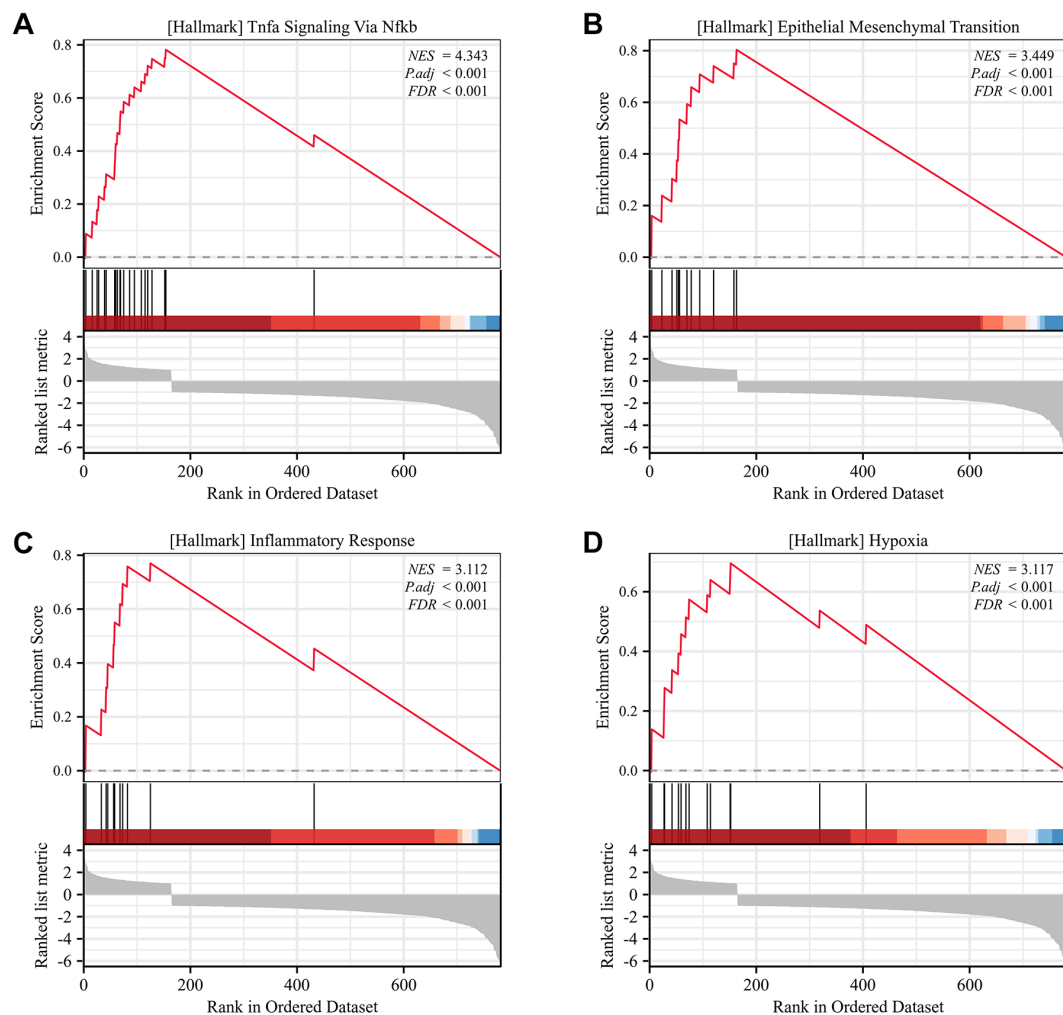

FIGURE 7
Gene Set Enrichment Analysis (GSEA) of SLC2A3 in KIRC. **(A)** Hallmark pathway of TNFα signaling via NF-κB. **(B)** Hallmark pathway of epithelial-mesenchymal transition (EMT). **(C)** Hallmark pathway of inflammatory response. **(D)** Hallmark pathway of hypoxia.
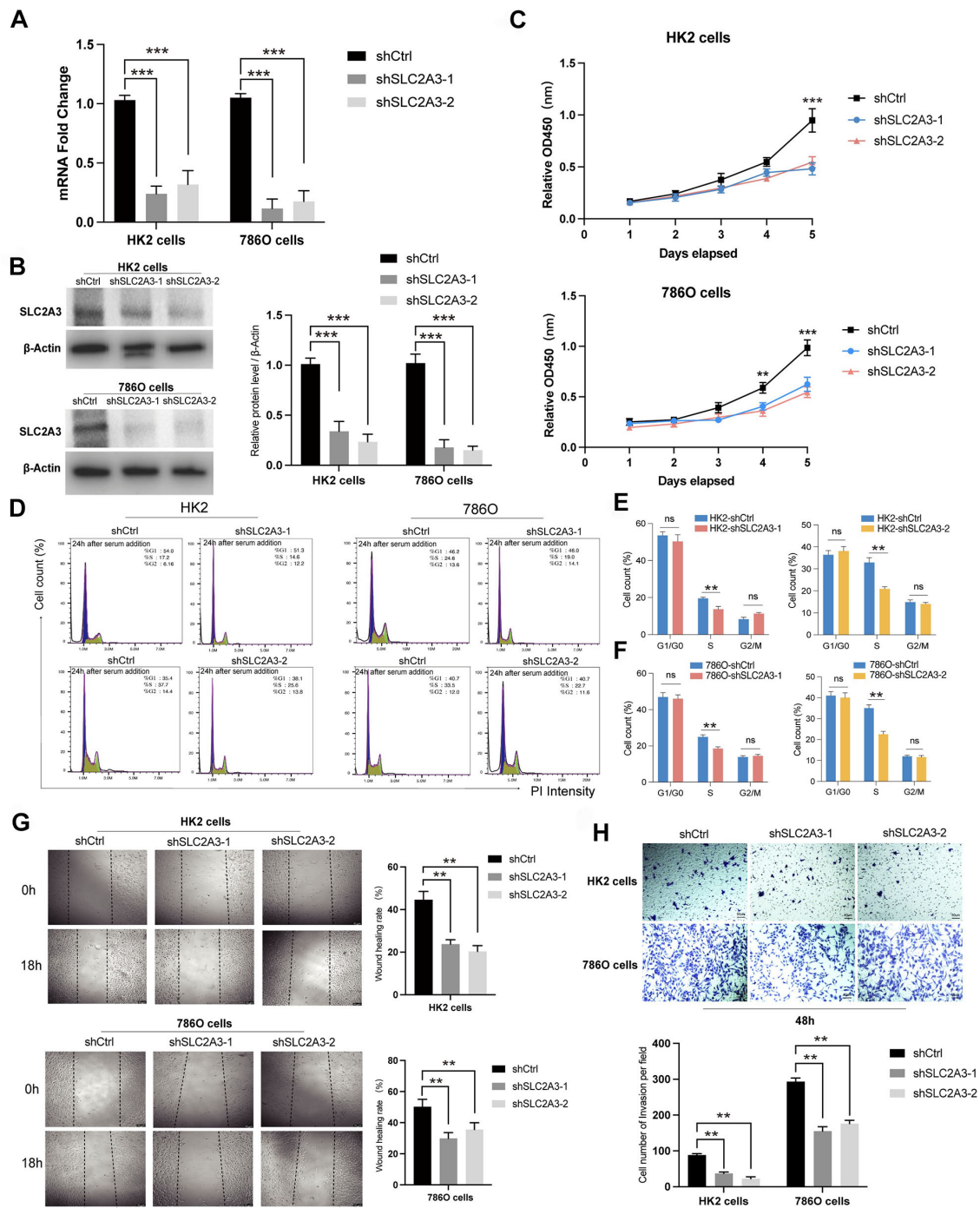
FIGURE 8

Functional validation of SLC2A3 knockdown in HK-2 and 786-O cells. **(A)** RT-qPCR results showing the knockdown efficiency of SLC2A3 in HK-2 and 786-O cells (n = 3 per group). **(B)** Western blotting analysis and grayscale quantification confirming SLC2A3 knockdown efficiency in HK-2 and 786-O cells (n = 3 per group). **(C)** CCK-8 assay results demonstrating decreased proliferation following SLC2A3 silencing in HK-2 and 786-O cells (n = 3 per group). **(D)** Flow cytometry analysis of the cell cycle in HK-2 and 786-O cells after SLC2A3 knockdown (n = 3 per group). **(E)** Quantification of cell cycle distribution in HK-2 cells (n = 3 per group). **(F)** Quantification of cell cycle distribution in 786-O cells (n = 3 per group). **(G)** Wound healing assay and quantification showing reduced migratory ability in HK-2 and 786-O cells after SLC2A3 silencing (scale bar: 50 μm) (n = 3 per group). **(H)** Transwell migration assay and quantification confirming impaired migration of HK-2 and 786-O cells after SLC2A3 knockdown (scale bar: 50 μm) (n = 3 per group).

resistance, highlighting the need for new therapeutic targets (8). As a key glucose transporter, SLC2A3 regulates cellular metabolism, energy homeostasis, and signal transduction in diverse cancer types, drawing increasing attention for its role in tumor biology (36, 37). In this study, we focused on SLC2A3 and demonstrated its contribution to tumor-associated biological processes.

One of the central challenges in oncology is the scarcity of reliable biomarkers and actionable targets (38, 39). Pan-cancer analysis indicates that SLC2A3 is aberrantly expressed across multiple tumor types and correlates with poor clinical outcomes, highlighting its potential as a universal marker of metabolic reprogramming and immune regulation in cancer. However, our data highlight that the functional implications of SLC2A3 are not entirely uniform across cancers. In bladder cancer, SLC2A3 functions as a risk stratification biomarker and shows strong associations with prognosis, immune landscape, and therapeutic response (40). Our previous work further identified five key SLC family genes, including SLC2A3, and developed a prognostic signature capable of predicting outcomes in KIRC patients (19). SLC2A3 exhibits significant prognostic value across various cancers, but its impact is highly tumor-type dependent. However, in certain cancers, such as PRAD and TARGET-ALL, low expression is linked to worse outcomes; similarly, in CHOL, low expression predicts poor PFI. This tumor-type specificity likely reflects functional differences of SLC2A3 across tissues and microenvironments. In most cancers, high SLC2A3 expression may drive glycolytic reprogramming and tumor proliferation, accelerating disease progression. In contrast, in tumors such as PRAD, CHOL, or TARGET-ALL, low SLC2A3 expression may be associated with tumor-specific metabolic dependencies or distinct immune microenvironment features, such as low glycolytic reliance, immune evasion mechanisms, or a more aggressive phenotype, resulting in poorer prognosis for patients with low expression (41).

Tumor heterogeneity, driven by genomic instability and cancer stemness, is a key determinant of therapeutic resistance, particularly to immunotherapy (42, 43). Our findings revealed that SLC2A3 expression is closely linked to genomic heterogeneity and tumor stemness, suggesting a role in modulating tumor adaptability under therapeutic pressure. Highly heterogeneous tumors frequently harbor diverse subclones, promoting immune escape and the development of resistant populations (44). Interestingly, contrary to the trend that SLC2A3 expression is positively correlated with TMB in most cancers, a negative correlation was observed in LIHC. This may reflect the unique metabolic and genetic landscape of liver tumors, including distinctive glucose and lipid metabolism as well as mutations in genes such as *CTNNB1* and *TP5*3 (45). In LIHC, high SLC2A3 expression may primarily reflect glycolytic reprogramming rather than genomic instability (46). Cancer stem-like cells possess enhanced DNA repair capabilities, self-renewal potential, and metabolic flexibility, contributing to both intrinsic and acquired resistance to immune checkpoint blockade (47). In glioblastoma, high SLC2A3 expression maintains the stem-like phenotype by increasing glycolytic activity, diminishing temozolomide cytotoxicity and leading to poor clinical outcomes (48). Similarly, in bladder cancer, SLC2A3 supports stemness

maintenance and tumor progression by meeting the metabolic demands of cancer cells (49). Our results indicate that inhibiting SLC2A3 may impair metabolic adaptation, decrease tumor heterogeneity and stemness, and improve responses to immunotherapy. Cutting-edge advances in single-cell sequencing and immunogenomics have unraveled the intricate complexity of the TIME (50, 51). In colorectal cancer, SLC2A3 expression positively correlates with CD4+ and CD8+ T-cell infiltration and modulates PD-L1 expression, thereby contributing to immune evasion (52). In HNSCC, SLC2A3 expression is negatively correlated with various immune cell types, suggesting it may promote tumor progression by suppressing anti-tumor immunity (53). Our analyses showed that SLC2A3 expression is strongly positively correlated with immune-related genes, including immune checkpoint molecules, stimulatory factors, chemokines, immunoinhibitors, and immune receptors, in most tumors, with negative correlations observed only in TGCT. Further evaluation of the tumor microenvironment revealed positive associations between SLC2A3 and StromalScore, ImmuneScore, and ESTIMATEScore, except in TGCT. Analysis of immune infiltration revealed that elevated SLC2A3 expression is generally linked to higher levels of macrophages, Th1/Th2 cells, and Tregs, while showing a negative correlation with Th17 cells. Additionally, SLC2A3 positively correlates with CD4 memory-activated T cells, M0 macrophages, activated mast cells, and neutrophils, but is inversely associated with Tregs, activated NK cells, and memory B cells. These results suggest that SLC2A3 may modulate tumor progression through its effects on the immune microenvironment.

In KIRC, the biological role of SLC2A3 exhibits significant tissue specificity. Unlike most solid tumors, the energy metabolism characteristics of KIRC are unique, mainly manifested as the continuous activation of HIF signaling due to *VHL* gene inactivation, which leads to the upregulation of glycolysis and the reprogramming of lipid metabolism (8). As a high-affinity glucose transporter, the overexpression of SLC2A3 may further enhance glucose uptake and glycolytic flux, providing an energy advantage for tumor cells in hypoxic environments (18, 46). Moreover, SLC2A3 expression is positively correlated with various innate and adaptive immune cells, as well as with key immune checkpoint molecules. These results suggest that SLC2A3 may contribute to the formation of an immune-infiltrated yet immunosuppressive tumor microenvironment. Clinically, high SLC2A3 expression could serve as a predictive biomarker for response to immune checkpoint inhibitor therapy. Mechanistically, SLC2A3 is often overexpressed in various cancers and facilitates tumor progression by enhancing glucose uptake and activating NF-κB/EMT signaling (53). In colorectal cancer, low-glucose conditions trigger SLC2A3 expression through the AMPK/CREB1 pathway, promoting both glucose absorption and cell proliferation (54). Its role in shaping the tumor immune microenvironment further supports its relevance as a prognostic biomarker and potential therapeutic target. Consistent with these observations, we found that high SLC2A3 expression in KIRC is associated with inflammatory responses, extracellular matrix remodeling, and activation of the NF-κB/EMT pathway.

Functional assays demonstrated that silencing SLC2A3 suppresses cell proliferation, cell cycle progression, and migration, indicating that SLC2A3 may drive KIRC progression through NF-κB/EMT-mediated mechanisms.

Nevertheless, several limitations warrant consideration. First, we lacked clinical samples to directly validate the relationship between SLC2A3 expression and patient outcomes, and functional verification was performed exclusively *in vitro*, without *in vivo* confirmation. Second, our analyses relied heavily on publicly available transcriptomic datasets, which may introduce biases such as cohort heterogeneity and batch effects. Third, immune infiltration estimates derived from deconvolution algorithms are based on predefined signature matrices and may not fully capture complex cellular interactions or rare cell populations. Finally, functional validation in cell lines may not fully recapitulate the heterogeneity and microenvironmental context of primary tumors. Therefore, while our results provide strong correlative evidence, causal mechanisms require further experimental verification, ideally using *in vivo* models.

Conclusions

SLC2A3 shows aberrant expression across multiple cancers and is strongly associated with patient outcomes, tumor heterogeneity, and immune microenvironment features. In RCC, it may drive cell proliferation and migration through pathways related to inflammation, EMT, and hypoxia.

Data availability statement

The original contributions presented in the study are included in the article/supplementary material. Further inquiries can be directed to the corresponding authors.

Ethics statement

Ethical approval was not required for the studies on humans in accordance with the local legislation and institutional requirements because only commercially available established cell lines were used.

Author contributions

ZL: Conceptualization, Data curation, Formal Analysis, Funding acquisition, Investigation, Software, Validation, Visualization, Writing – original draft, Writing – review & editing. XZ: Data curation, Formal Analysis, Investigation, Methodology, Supervision, Writing – original draft, Writing – review & editing. HY: Investigation, Methodology, Project administration, Writing – review & editing. QY: Formal Analysis, Investigation, Methodology, Project administration, Resources, Writing – review & editing. YY: Formal Analysis, Investigation, Methodology, Project administration, Resources, Writing – review & editing. ZZ: Formal Analysis, Investigation, Methodology, Project administration, Resources, Writing – review & editing. GW: Investigation, Methodology, Formal analysis, Project administration, Resources, Writing – review & editing. LB: Conceptualization, Data curation, Formal Analysis, Funding acquisition, Investigation, Project administration, Resources, Supervision, Writing – original draft, Writing – review & editing.

Funding

Conflict of interest

The authors declare that the research was conducted in the absence of any commercial or financial relationships that could be construed as a potential conflict of interest.

Generative AI statement

The author(s) declare that no Generative AI was used in the creation of this manuscript.

Any alternative text (alt text) provided alongside figures in this article has been generated by Frontiers with the support of artificial intelligence and reasonable efforts have been made to ensure accuracy, including review by the authors wherever possible. If you identify any issues, please contact us.

Publisher's note

References

1. Wu M, Liao Y, Tang L. Non-small cell lung cancer organoids: Advances and challenges in current applications. *Chin J Cancer Res*. (2024) 36:455–73. doi: 10.21147/j.issn.1000-9604.2024.05.01

2. Bray F, Laversanne M, Sung H, Ferlay J, Siegel RL, Soerjomataram I, et al. Global cancer statistics 2022: GLOBOCAN estimates of incidence and mortality worldwide for 36 cancers in 185 countries. *CA Cancer J Clin*. (2024) 74:229–63. doi: 10.3322/caac.21834

3. Feng DC, Li DX, Wu RC, Wang J, Xiao YH, Yoo KH, et al. Global burden and cross-country inequalities in urinary tumors from 1990 to 2021 and predicted incidence changes to 2046. *Mil Med Res*. (2025) 12:12. doi: 10.1186/s40779-025-00599-y

4. Wu Z, Xia F, Lin R. Global burden of cancer and associated risk factors in 204 countries and territories, 1980-2021: a systematic analysis for the GBD 2021. *J Hematol Oncol*. (2024) 17:119. doi: 10.1186/s13045-024-01640-8

5. Zhou F, Huang L, Li S, Yang W, Chen F, Cai Z, et al. From structural design to delivery: mRNA therapeutics for cancer immunotherapy. *Explor (Beijing)*. (2024) 4:20210146. doi: 10.1002/EXP.20210146

6. Qin L, Liang T, Zhu X, Hu W, Li B, Wei M, et al. Senescent macrophages and the lung cancer microenvironment: A new perspective on tumor immune evasion. *Aging Dis*. (2024) 16:3453–65. doi: 10.14336/AD.2024.1404

7. Hu A, Sun L, Lin H, Liao Y, Yang H, Mao Y. Harnessing innate immune pathways for therapeutic advancement in cancer. *Signal Transduct Target Ther*. (2024) 9:68. doi: 10.1038/s41392-024-01765-9

8. Young M, Jackson-Spence F, Beltran L, Day E, Suarez C, Bex A, et al. Renal cell carcinoma. *Lancet*. (2024) 404:476–91. doi: 10.1016/S0140-6736(24)00917-6

9. Barragan-Carrillo R, Saad E, Saliby RM, Sun M, Albiges L, Bex A, et al. First and second-line treatments in metastatic renal cell carcinoma. *Eur Urol*. (2025) 87:143–54. doi: 10.1016/j.eururo.2024.10.019

10. Catalano M, Procopio G, Sepe P, Santoni M, Sessa F, Villari D, et al. Tyrosine kinase and immune checkpoints inhibitors in favorable risk metastatic renal cell carcinoma: Trick or treat? *Pharmacol Ther*. (2023) 249:108499. doi: 10.1016/j.pharmthera.2023.108499

11. Marona P, Górka J, Kwapisz O, Jura J, Rys J, Hoffman RM, et al. Resistance to tyrosine kinase inhibitors promotes renal cancer progression through MCPIP1 tumor-suppressor downregulation and c-Met activation. *Cell Death Dis*. (2022) 13:814. doi: 10.1038/s41419-022-05251-4

12. Gulati S, Barata PC, Elliott A, Bilen MA, Burgess EF, Choueiri TK, et al. Molecular analysis of primary and metastatic sites in patients with renal cell carcinoma. *J Clin Invest*. (2024) 134:e176230. doi: 10.1172/JCI176230

13. Rioja P, Rey-Cardenas M, De Velasco G. Targeting HIF-2α and anemia: A therapeutic breakthrough for clear-cell renal cell carcinoma. *Cancer Treat Rev*. (2024) 129:102801. doi: 10.1016/j.ctrv.2024.102801

14. Khan A, Liu Y, Gad M, Kenny TC, Birsoy K. Solute carriers: The gatekeepers of metabolism. *Cell*. (2025) 188:869–84. doi: 10.1016/j.cell.2025.01.015

15. Sun LL, He HY, Li W, Jin WL, Wei YJ. The solute carrier transporters (SLCs) family in nutrient metabolism and ferroptosis. *biomark Res*. (2024) 12:94. doi: 10.1186/s40364-024-00645-2

16. Yoo HC, Park SJ, Nam M, Kang J, Kim K, Yeo JH, et al. A variant of SLC1A5 is a mitochondrial glutamine transporter for metabolic reprogramming in cancer cells. *Cell Metab*. (2020) 31:267–83. doi: 10.1016/j.cmet.2019.11.020

17. Zhang J, Sjøberg KA, Gong S, Wang T, Li F, Kuo A, et al. Endothelial metabolic control of insulin sensitivity through resident macrophages. *Cell Metab*. (2024) 36:2383–401. doi: 10.1016/j.cmet.2024.08.008

18. Jiang W, Xu S, Li P. SLC2A3 is a potential factor for head and neck squamous cancer development through tumor microenvironment alteration. *Curr Gene Ther*. (2025) 25:157–77. doi: 10.2174/0115665232291300240509104344

19. Wen H, Dai F, Wang H, Lin Y, Xu Z, Lyu Z. Identification and validation of SLC16A8 as a prognostic biomarker in clear cell renal cell carcinoma: a six-gene solute carrier signature. *Exp Cell Res*. (2025) 448:114567. doi: 10.1016/j.yexcr.2025.114567

20. Liu J, Hong J, Han H, Park J, Kim D, Park H, et al. Decreased vitamin C uptake mediated by SLC2A3 promotes leukaemia progression and impedes TET2 restoration. *Br J Cancer*. (2020) 122:1445–52. doi: 10.1038/s41416-020-0788-8

21. Goldman MJ, Craft B, Hastie M, Repečka K, McDade F, Kamath A, et al. Visualizing and interpreting cancer genomics data via the Xena platform. *Nat Biotechnol*. (2020) 38:675–78. doi: 10.1038/s41587-020-0546-8

22. Wu P, Lin Y, Dai F, Wang H, Wen H, Xu Z, et al. Pan-cancer analysis and experimental validation revealed the prognostic role of ZNF83 in renal and lung cancer cohorts. *Discov Oncol*. (2025) 16:1335. doi: 10.1007/s12672-025-03026-9

23. Chen D, Xu L, Xing H, Shen W, Song Z, Li H, et al. Sangerbox 2: Enhanced functionalities and update for a comprehensive clinical bioinformatics data analysis platform. *Imeta*. (2024) 3:e238. doi: 10.1002/imt2.238

24. Thorsson V, Gibbs DL, Brown SD, Wolf D, Bortone DS, Ou YT, et al. The immune landscape of cancer. *Immunity*. (2018) 48:812–30. doi: 10.1016/j.immuni.2018.03.023

25. Bonneville R, Krook MA, Kautto EA, Miya J, Wing MR, Chen HZ, et al. Landscape of microsatellite instability across 39 cancer types. *Jco Precis Oncol*. (2017) 2017:PO.17.00073. doi: 10.1200/PO.17.00073

26. Mayakonda A, Lin DC, Assenov Y, Plass C, Koeffler HP. Maftools: efficient and comprehensive analysis of somatic variants in cancer. *Genome Res*. (2018) 28:1747–56. doi: 10.1101/gr.239244.118

27. Malta TM, Sokolov A, Gentles AJ, Burzykowski T, Poisson L, Weinstein JN, et al. Machine learning identifies stemness features associated with oncogenic dedifferentiation. *Cell*. (2018) 173:338–54. doi: 10.1016/j.cell.2018.03.034

28. Liao C, Wang X. TCGAplot: an R package for integrative pan-cancer analysis and visualization of TCGA multi-omics data. *BMC Bioinf*. (2023) 24:483. doi: 10.1186/s12859-023-05615-3

29. Newman AM, Liu CL, Green MR, Gentles AJ, Feng W, Xu Y, et al. Robust enumeration of cell subsets from tissue expression profiles. *Nat Methods*. (2015) 12:453–57. doi: 10.1038/nmeth.3337

30. Hänzelmann S, Castelo R, Guinney J. GSVA: gene set variation analysis for microarray and RNA-seq data. *BMC Bioinf*. (2013) 14:7. doi: 10.1186/1471-2105-14-7

31. Wu T, Hu E, Xu S, Chen M, Guo P, Dai Z, et al. clusterProfiler 4.0: A universal enrichment tool for interpreting omics data. *Innovation (Camb)*. (2021) 2:100141. doi: 10.1016/j.xinn.2021.100141

32. Liberzon A, Birger C, Thorvaldsdóttir H, Ghandi M, Mesirov JP, Tamayo P. The Molecular Signatures Database (MSigDB) hallmark gene set collection. *Cell Syst*. (2015) 1:417–25. doi: 10.1016/j.cels.2015.12.004

33. Livak KJ, Schmittgen TD. Analysis of relative gene expression data using real-time quantitative PCR and the 2(-Delta Delta C(T)) Method. *Methods*. (2001) 25:402–08. doi: 10.1006/meth.2001.1262

34. Bai F, Deng Y, Li L, Lv M, Razzokov J, Xu Q, et al. Advancements and challenges in brain cancer therapeutics. *Explor (Beijing)*. (2024) 4:20230177. doi: 10.1002/EXP.20230177

35. Singh M, Morris VK, Bandey IN, Hong DS, Kopetz S. Advancements in combining targeted therapy and immunotherapy for colorectal cancer. *Trends Cancer*. (2024) 10:598–609. doi: 10.1016/j.trecan.2024.05.001

36. Yao W, Shang L, Wang Y, Xu L, Bai Y, Feng M, et al. DNMT1-driven methylation of RORA facilitates esophageal squamous cell carcinoma progression under hypoxia through SLC2A3. *J Transl Med*. (2024) 22:1167. doi: 10.1186/s12967-024-05960-8

37. Yan B, Li X, Peng M, Zuo Y, Wang Y, Liu P, et al. The YTHDC1/GLUT3/RNF183 axis forms a positive feedback loop that modulates glucose metabolism and bladder cancer progression. *Exp Mol Med*. (2023) 55:1145–58. doi: 10.1038/s12276-023-00997-z

38. Yang Y, Liang J, Zhao J, Wang X, Feng D, Xu H, et al. The multi-omics analyses of acsl1 reveal its translational significance as a tumor microenvironmental and prognostic biomarker in clear cell renal cell carcinoma. *Diagn Pathol*. (2023) 18:96. doi: 10.1186/s13000-023-01384-y

39. Tian B, Pang Y, Gao Y, Meng Q, Xin L, Sun C, et al. A pan-cancer analysis of the oncogenic role of Golgi transport 1B in human tumors. *J Transl Int Med*. (2023) 11:433–48. doi: 10.2478/jtim-2023-0002

40. Sun M, Zhang Q, He Z, Luo Y, Tu Y, Peng L, et al. Integrated multiomics analysis and machine learning approaches in bladder cancer: unveiling the impact of immunogenic cell death and its key gene SLC2A3 on prognosis and personalized treatment strategies. *ACS Omega*. (2025) 10:24655–74. doi: 10.1021/acsomega.5c01496

41. Vaz CV, Marques R, Alves MG, Oliveira PF, Cavaco JE, Maia CJ, et al. Androgens enhance the glycolytic metabolism and lactate export in prostate cancer cells by modulating the expression of GLUT1, GLUT3, PFK, LDH and MCT4 genes. *J Cancer Res Clin Oncol*. (2016) 142:5–16. doi: 10.1007/s00432-015-1992-4

42. Tuo Z, Zhang Y, Li D, Wang Y, Wu R, Wang J, et al. Relationship between clonal evolution and drug resistance in bladder cancer: A genomic research review. *Pharmacol Res*. (2024) 206:107302. doi: 10.1016/j.phrs.2024.107302

43. Holder AM, Dedeilia A, Sierra-Davidson K, Cohen S, Liu D, Parikh A, et al. Defining clinically useful biomarkers of immune checkpoint inhibitors in solid tumours. *Nat Rev Cancer*. (2024) 24:498–512. doi: 10.1038/s41568-024-00705-7

44. Grassi E, Vurchio V, Cresswell GD, Catalano I, Lupo B, Sassi F, et al. Heterogeneity and evolution of DNA mutation rates in microsatellite stable colorectal cancer. *Sci Transl Med*. (2025) 17:eado1641. doi: 10.1126/scitranslmed.ado1641

45. Murai H, Kodama T, Maesaka K, Tange S, Motooka D, Suzuki Y, et al. Multiomics identifies the link between intratumor steatosis and the exhausted tumor immune microenvironment in hepatocellular carcinoma. *Hepatology*. (2023) 77:77–91. doi: 10.1002/hep.32573

46. Ribeiro KS, Karmakar E, Park C, Garg R, Kung GP, Kadakia I, et al. Iron regulates cellular proliferation by enhancing the expression of glucose transporter GLUT3 in the liver. *Cells*. (2024) 13:1147. doi: 10.3390/cells13131147

47. Verona F, Di Bella S, Schirano R, Manfredi C, Angeloro F, Bozzari G, et al. Cancer stem cells and tumor-associated macrophages as mates in tumor progression:

mechanisms of crosstalk and advanced bioinformatic tools to dissect their phenotypes and interaction. *Front Immunol*. (2025) 16:1529847. doi: 10.3389/fimmu.2025.1529847

48. Ho KH, Chen PH, Chou CM, Shih CM, Lee YT, Cheng CH, et al. A key role of DNA damage-inducible transcript 4 (DDIT4) connects autophagy and GLUT3-mediated stemness to desensitize temozolomide efficacy in glioblastomas. *Neurotherapeutics*. (2020) 17:1212–27. doi: 10.1007/s13311-019-00826-0

49. Ma L, Chen H, Yang W, Ji Z. Crosstalk between mesenchymal stem cells and cancer stem cells reveals a novel stemness-related signature to predict prognosis and immunotherapy responses for bladder cancer patients. *Int J Mol Sci*. (2023) 24:4760. doi: 10.3390/ijms24054760

50. Feng DC, Zhu WZ, Wang J, Li DX, Shi X, Xiong Q, et al. The implications of single-cell RNA-seq analysis in prostate cancer: unraveling tumor heterogeneity, therapeutic implications and pathways towards personalized therapy. *Mil Med Res*. (2024) 11:21. doi: 10.1186/s40779-024-00526-7

51. González-Martínez S, Pérez-Mies B, Cortés J, Palacios J. Single-cell RNA sequencing in endometrial cancer: exploring the epithelial cells and the microenvironment landscape. *Front Immunol*. (2024) 15:1425212. doi: 10.3389/fimmu.2024.1425212

52. Gao H, Liang J, Duan J, Chen L, Li H, Zhen T, et al. A prognosis marker SLC2A3 correlates with EMT and immune signature in colorectal cancer. *Front Oncol*. (2021) 11:638099. doi: 10.3389/fonc.2021.638099

53. Chai F, Zhang J, Fu T, Jiang P, Huang Y, Wang L, et al. Identification of SLC2A3 as a prognostic indicator correlated with the NF-κB/EMT axis and immune response in head and neck squamous cell carcinoma. *Channels (Austin)*. (2023) 17:2208928. doi: 10.1080/19336950.2023.2208928

54. Dai W, Xu Y, Mo S, Li Q, Yu J, Wang R, et al. GLUT3 induced by AMPK/CREB1 axis is key for withstanding energy stress and augments the efficacy of current colorectal cancer therapies. *Signal Transduct Target Ther*. (2020) 5:177. doi: 10.1038/s41392-020-00220-9